

Voltage-driven perpendicular magnetic domain switching in multiferroic nanoislands

Jia-Mian Hu, T. N. Yang, L. Q. Chen, and C. W. Nan

Citation: *J. Appl. Phys.* **113**, 194301 (2013); doi: 10.1063/1.4804157

View online: <http://dx.doi.org/10.1063/1.4804157>

View Table of Contents: <http://jap.aip.org/resource/1/JAPIAU/v113/i19>

Published by the **AIP Publishing LLC**.

Additional information on *J. Appl. Phys.*

Journal Homepage: <http://jap.aip.org/>

Journal Information: http://jap.aip.org/about/about_the_journal

Top downloads: http://jap.aip.org/features/most_downloaded

Information for Authors: <http://jap.aip.org/authors>

ADVERTISEMENT



AIP Advances

Now Indexed in Thomson Reuters Databases

Explore AIP's open access journal:

- Rapid publication
- Article-level metrics
- Post-publication rating and commenting

Voltage-driven perpendicular magnetic domain switching in multiferroic nanoislands

Jia-Mian Hu,^{1,a)} T. N. Yang,² L. Q. Chen,^{1,2} and C. W. Nan^{1,a)}

¹*School of Materials Science and Engineering and State Key Lab of New Ceramics and Fine Processing, Tsinghua University, Beijing 100084, China*

²*Department of Materials Science and Engineering, Pennsylvania State University, University Park, Pennsylvania 16802, USA*

(Received 6 March 2013; accepted 22 April 2013; published online 15 May 2013)

We show that, using phase-field simulations, large voltage-driven perpendicular magnetic domain switching can be realized in magnetic-ferroelectric nanoislands with relieved substrate constraint, which is difficult in continuous multiferroic layered thin films due to significant substrate clamping. The as-grown magnetic and ferroelectric domain structures in the heterostructured nanoislands can be tailored by engineering their respective geometric sizes and/or the underlying substrate strain. Influences of the lateral size of the island on the dynamic voltage-driven magnetic domain switching are addressed, whereby an optimum lateral size is identified for illustration. Thus, such three-dimensional multiferroic nanoislands should provide great flexibilities for designing novel high-density spintronic/microelectronic devices with purely voltage-driven means. © 2013 AIP Publishing LLC. [<http://dx.doi.org/10.1063/1.4804157>]

I. INTRODUCTION

A big problem for the on-chip integration and subsequent miniaturization of magnetic devices (e.g., memories, sensors, and oscillators) is the necessity of using Ampère-current-induced magnetic field to drive the magnetization/magnetic domain states,^{1–3} which is slow, power-consuming, and difficult to contain locally when the device component becomes small.⁴ The latter would in turn increase the current densities per unit area and cause severe heat dissipation. Spin current driven domain switching^{5,6} might be promising because of its benign scalability, i.e., the writing current decreases with shrinking size of the cross-sectional area in the device structure, but its high threshold current is another issue.⁷ In this case, switching magnetic domain directly using electric-voltage (field) could be the ultimate solution in reducing the energy cost due to the ideal zero current flow.⁸

Such voltage-driven magnetization/magnetic domain switching has been observed in single thin films of diluted magnetic semiconductors at low temperature⁹ and in ultrathin (several monolayers) transitional magnets with high triggering electric(E)-fields (10^5 MV/m or above).¹⁰ For practical applications, a low E -field and room-temperature operation is preferred, which has been achieved in multiferroic (e.g., artificially combined magnetic-ferroelectric) heterostructures^{11–13} via electrically modulated changes in spin-polarized charge,¹⁴ interfacial orbital configuration (e.g., hybridization^{15,16} and reconstruction^{17–19}), strain transfer,^{20,21} and/or exchange bias.^{22,23} However, existing research efforts have mostly been focused on continuous multiferroic thin films grown on a substrate while patterned multiferroic composite nanoislands [Fig. 1(a)] of technological importance have not been explored.

In this article, we studied, using phase-field simulations,^{24,25} the voltage-driven magnetic domain switching in a magnetic-ferroelectric (FE) heterostructured nanoisland grown on a substrate. Details about the phase-field simulations of the FE and magnetic phase transitions and corresponding domain structures are described in Sec. II. Such an island structure is an ideal prototype for high-performance, electrically actuated spintronic devices [e.g., see the patterned bits in Fig. 1(a)]: first, its small size is a pre-requisite for nanoscale devices with high densities;²⁶ second, relieved lateral constraint in a FE island allows large electromechanical strains originating from the ferroelastic $a_1(a_2)$ to c domain switching²⁷ (normally one or two orders of magnitude larger than the linear piezostain), which should be sufficient to overcome the strong out-of-plane demagnetization field and induce a 90° perpendicular domain switching in the upper magnetic layer²⁸ via strain transfer across the interface. It is worth pointing out that the electromechanical strains would be considerably smaller in a continuous FE thin film due to the remarkable substrate clamping²⁹ which also increases the propensity of ferroelastic relaxation³⁰ and destroy the established strain state accordingly. In addition, such ferroelastic strains are hard to be recoverable (i.e., the initial strain states would hardly restore after removing the voltage)³¹ in stress-free bulk ferroelectrics wherein significant fatigue would happen as well after repeated poling. We schematically show in Sec. III, the heterostructured nanoislands and corresponding patterned-bit array with relieved substrate constraint. As-grown magnetic and ferroelectric domain structures are also presented, which can be tailored by engineering their respective geometric sizes and/or the underlying substrate strain. We further discuss the voltage-driven perpendicular magnetic domain switching in such nanoislands of various lateral sizes (length and width, assumed to be equal herein) in Sec. IV. An optimum lateral size which can ensure both a large voltage-induced magnetic

^{a)}Authors to whom correspondence should be addressed. Electronic addresses: hjm08@mails.tsinghua.edu.cn and cwnan@tsinghua.edu.cn.

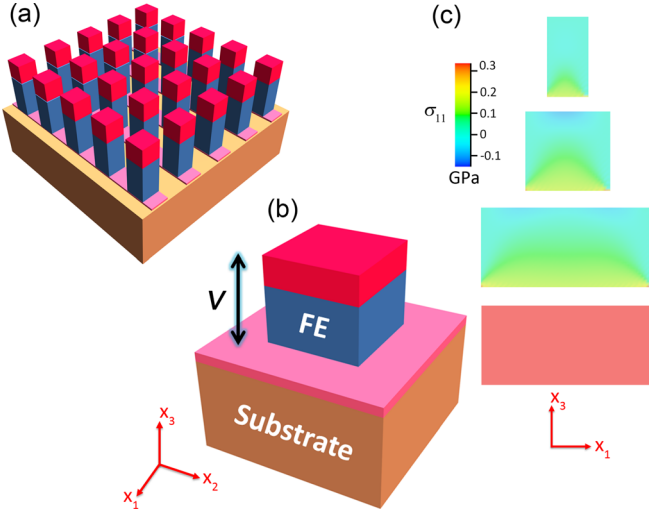


FIG. 1. Schematics of (a) the high-density patterned bit array and (b) the building block, i.e., a multiferroic nanoisland grown on a substrate. An electric-voltage (V) is applied perpendicularly to the ferroelectric (FE) layer between the top magnetic layer and the bottom electrode. (c) The in-plane stress distribution σ_{11} along the cross section at the center of FE island: (from top to bottom) $32 \times 32 \times 60 \text{ nm}^3$, $64 \times 64 \times 60 \text{ nm}^3$, $128 \times 128 \times 60 \text{ nm}^3$, and a fully constrained FE thin film. The biaxial strain from the substrate is taken as (0.2%, 0.2%).

domain switching and high density of the patterned bit array is identified for illustration.

II. PHASE-FIELD MODEL

In the phase-field approach, the magnetic and FE domain structures are represented by the spatial distributions of the local magnetization vectors $\mathbf{M} = M_s \mathbf{m} = M_s(m_1, m_2, m_3)$ and local polarization vectors $\mathbf{P} = (P_1, P_2, P_3)$, where M_s and $m_i (i = 1, 2, 3)$ represent the saturation magnetization and the direction cosine, respectively.

For the FE layer in the present multiferroic island, the temporal domain structure evolution is described by the time-dependent Ginzburg-Landau equation (TDGL),

$$\frac{\partial P_i}{\partial t} = -L \frac{\delta F_p}{\delta P_i} \quad (i = 1, 2, 3), \quad (1)$$

where L is a kinetic coefficient that is related to the domain evolution and F_p is the total free energy of the ferroelectrics that can be expressed as,

$$F_p = F_{bulk}(\mathbf{P}) + F_{wall}(\mathbf{P}) + F_{elec}(\mathbf{P}, \mathbf{E}) + F_{elas}(\mathbf{P}, \boldsymbol{\varepsilon}), \quad (2)$$

where F_{bulk} , F_{wall} , F_{elec} , F_{elas} are bulk free energy, domain wall energy, electrostatic energy, and elastic energy, respectively. The electrostatic energy of a given polarization distribution is given by,³²

$$F_{elec}(\mathbf{P}, \mathbf{E}) = \int - (1/2)^* E_i^* \kappa_0^* \kappa_{ij}^* E_j - (E_i^* P_i) dV \quad (i = 1, 2, 3), \quad (3)$$

where κ_0 (κ_{ij}) denotes the vacuum (relative) dielectric permittivity and E_i is the electric field component. It comprises an applied electric field E_i^a that depends on the electric potentials that are specified on both the top and bottom

surfaces of the FE island, and a depolarization field E_i^d , which is determined by the polarization distribution and the electrical (electrostatic) boundary conditions.^{32,33} A short-circuit electrical boundary condition, i.e., the polarization charges are compensated, is applied on the top and bottom surfaces of the island herein upon the application of a perpendicular voltage bias [Fig. 1(b)], while open-circuit boundary conditions are set on the lateral surfaces wherein the uncompensated charges along the lateral surfaces should generate significant depolarization fields accordingly. The elastic energy in the ferroelectrics is

$$F_{elas}(\mathbf{P}, \boldsymbol{\varepsilon}) = \frac{1}{2} \int c_{ijkl} e_{ij} e_{kl} dV = \frac{1}{2} \int c_{ijkl} (\varepsilon_{ij} - \varepsilon_{ij}^0) (\varepsilon_{kl} - \varepsilon_{kl}^0) dV, \quad (4)$$

where the summation convention is employed and $i, j, k, l = 1, 2, 3$. c_{ijkl} is the elastic stiffness tensor, e_{ij} is the elastic strain, and $\varepsilon_{ij}^0 = Q_{ijkl} P_k P_l$ is the stress-free strain or structural (e.g., ferroelastic) transformation strain with Q_{ijkl} representing the electrostrictive coefficient. All the strain components as well as magnetization/polarization vectors are defined in a rectangular coordinate system $\mathbf{x} = (x_1, x_2, x_3)$ with the x_1 , x_2 , and x_3 axes along the three $[100]_p$, $[010]_p$, and $[001]_p$ crystal axes. The elastic energy solution for Eq. (4) is based on a previously developed model for such an isolated FE island³⁴ that was represented by three phases, i.e., a gas, an island, and a substrate, and the stress-free elastic boundary conditions along the island surfaces can be automatically satisfied by taking the elastic constants as zero for the gas phase. The average in-plane strain ε_{11} (or ε_{22}) within the FE island can then be calculated by solving Eq. (4), which is further transferred to the upper magnetic layer and drives the magnetic domain switching accordingly. The mathematic expressions for F_{bulk} and F_{wall} are the same as those given in Ref. 35.

The temporal evolution of the magnetization configuration and thus the magnetic domain structure is governed by the Landau-Lifshitz-Gilbert (LLG) equation, i.e.,

$$(1 + \alpha^2) \frac{\partial \mathbf{M}}{\partial t} = -\gamma_0 \mathbf{M} \times \mathbf{H}_{eff} - \frac{\gamma_0 \alpha}{M_s} \mathbf{M} \times (\mathbf{M} \times \mathbf{H}_{eff}), \quad (5)$$

where γ_0 is the gyromagnetic ratio calculated as $-2.2 \times 10^5 \text{ m/(A} \cdot \text{Sec)}$ by taking a g -factor of about 2.087 estimated from Ref. 36, α is the damping constant around 0.0054,³⁷ and \mathbf{H}_{eff} is the effective magnetic field, given as $\mathbf{H}_{eff} = -(1/\mu_0 M_s) (\delta F_m / \delta \mathbf{m})$. Here, μ_0 denotes the vacuum permeability and F_m is the total free energy of a (001) magnetic film upon no external magnetic field, expressed by,

$$F_m = F_{mc}(\mathbf{M}) + F_{ms}(\mathbf{M}) + F_{ex}(\mathbf{M}) + F_{elas}(\mathbf{M}, \boldsymbol{\varepsilon}), \quad (6)$$

where F_{mc} , F_{ms} , F_{ex} , F_{elas} are the magnetocrystalline, magnetostatic, exchange, and elastic energy, respectively. The elastic energy can be expressed in a similar way as Eq. (4), but using the elastic constants of the magnets and a different stress-free strain ε_{ij}^0 associated with the local magnetization change, i.e.,

$$\varepsilon_{ij}^0 = \frac{3}{2}\lambda_{100}\left(m_i m_j - \frac{1}{3}\right) \quad (i=j) \quad \text{or} \quad \frac{3}{2}\lambda_{111}m_i m_j \quad (i \neq j), \quad (7)$$

where λ_{100} and λ_{111} are the magnetostrictive constants. The magnetic layer is intimately attached to the bottom ferroelectrics and thus is subjected to a mixed elastic boundary condition for regular film-on-substrate system,²⁵ and the corresponding elastic energy can be calculated by combining Khachatryan's theory³⁸ with the Stroh's formalism of anisotropic elasticity.³⁹ The details for obtaining F_{mc} , F_{ms} , and F_{ex} are given in Ref. 40. To incorporate the influence of geometric size on the domain structures of such three-dimensional thin-film nanomagnets, a finite-size-magnet magnetostatic boundary condition is applied herein for obtaining F_{ms} .^{41,42}

The temporal evolution of the magnetic and FE domain structures in such a multiferroic island can thus be obtained by separately solving the LLG and TDGL equations, respectively, using the semi-implicit Fourier spectral method.⁴³ The FE island-on-substrate system is discretized into a three-dimensional array of cubic cells of $128\Delta x \times 128\Delta y \times 80\Delta z$. The thicknesses of the substrate and FE islands are set as $h_s = 25\Delta z$ and $h_f = 40\Delta z$, respectively. Among the upper cells of $128\Delta x \times 128\Delta y \times 40\Delta z$, only one fourth of them (i.e., $64\Delta x \times 64\Delta y \times 40\Delta z$) are occupied by the FE island, while the rest are the gas which allows the lateral relaxation of the island. On the other hand, a model size of $32\Delta x \times 32\Delta y \times 20\Delta z$ is employed to describe the domain structure evolution in the magnetic thin film. By varying the simulation system size and/or the grid size of each unit cell in real space, magnetic and FE layers with different geometric sizes can then be treated.^{27,40} The as-grown magnetic and FE domain structures (shown shortly later in Fig. 2) are stabilized from initial random magnetization and polarization distributions. After then, a perpendicular triangular-wave voltage of around 0.013 GHz is applied to the FE islands, i.e., the perpendicular electric field (voltage) E_3^a (V) varies by 1 MV/m (i.e., 0.06 V for a 60 nm FE island) successively every 10000 steps with a normalized time step $\Delta\tau = 0.002$ (around 0.48 ns in real time), which generates an average in-plane electromechanical strain ε_{11} almost instantaneously. The ε_{11} would be further used as the input for obtaining a magnetic domain structure within exactly the same time steps in order to simulate an *in-situ* voltage-driven dynamic magnetic domain evolution, although such a short time period (i.e., 0.48 ns) might be insufficient to obtain a stable magnetic or even FE domain structure in some cases as will be discussed later.

III. AS-GROWN MAGNETIC AND FERROELECTRIC DOMAIN STRUCTURES IN A MULTIFERROIC NANOISLAND

Figure 1(a) shows one typical patterned bit array design for high-density devices. The building block is a magnetic-FE heterostructured nanoisland [Fig. 1(b)]. The key feature of such an island structure is the relief of the mechanical constraint imposed by the stiff substrate. For illustration,

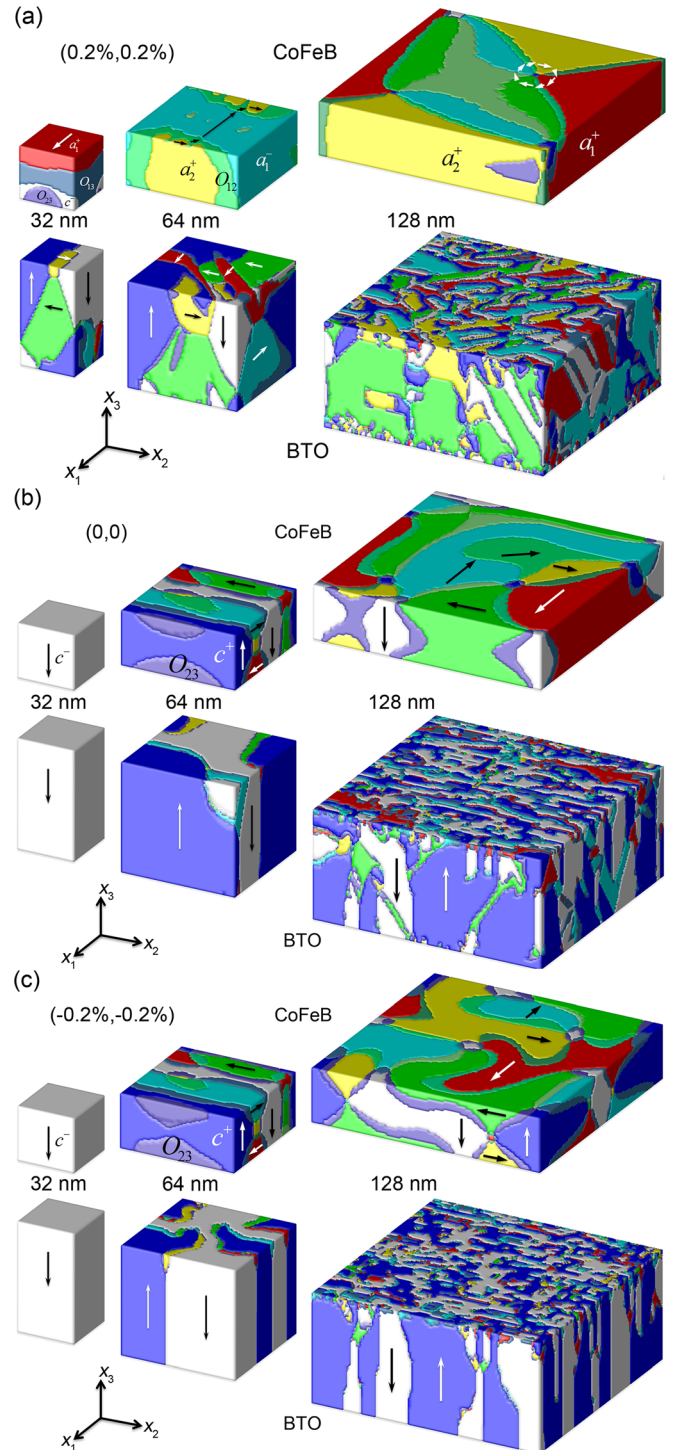


FIG. 2. Typical magnetic (the first row) and ferroelectric (FE) (the second row) domain structures in as-grown multiferroic $\text{Co}_{20}\text{Fe}_{60}\text{B}_{20}$ (CoFeB)/ BaTiO_3 (BTO) nanoislands under the substrate-imposed (a) tensile strain of (0.2%, 0.2%), (b) (0,0), and (c) compressive strain of (-0.2%, -0.2%). The lateral size (length and width) of both the magnetic and FE layers varies from $32 \times 32 \text{ nm}^2$ to $128 \times 128 \text{ nm}^2$. The thicknesses of the CoFeB and BTO are 30 nm and 60 nm, respectively. Each color and corresponding arrow represent one specific magnetic or FE domain orientation, where the same color scheme and notation (e.g., a , c , O) are used for simplicity.

Figure 1(c) shows the in-plane stress σ_{11} distribution (σ_{22} has a similar dependence) at the center of the FE island whose lateral size varies from 32 nm to 128 nm, but with the same thickness of 60 nm. Herein the spontaneous

polarization is set as zero (i.e., a paraelectric phase) for simplicity. Compared to a continuous thin film fully constrained on a substrate [i.e., the bottom plot in Fig. 1(c)], the in-plane stress σ_{11} exhibits a gradient distribution in FE islands with relaxed substrate constraint due to the stress-free boundary conditions along the surfaces of an isolated island, although the part close to the bottom substrate is still somewhat clamped. Moreover, the fraction of such clamped area gradually decreases with shrinking lateral size (e.g., the island of $32 \times 32 \times 60 \text{ nm}^3$) under the given thickness of 60 nm, indicating a more remarkable stress relaxation. Such relief of substrate clamping allows the presence of huge electromechanical strains from ferroelastic domain switching,²⁷ and such strains can be modulated by engineering both the aspect ratio of the island and the substrate strain as will be discussed later. Furthermore, the thickness of the upper magnetic film is taken to be 30 nm which is half of the FE island to ensure an effective strain transfer across the FE/magnetic interface.⁴⁴ In addition, it is worth noting that the fraction of the clamped area in FE islands would also decrease (increase) when increasing (reducing) the island thickness under a given lateral size and would result in an almost negligible substrate constraint (i.e., the average σ_{11} becomes almost zero) when the thickness exceeds a certain critical value. However, the critical thickness should vary with the lateral size and the strength of corresponding substrate constraint. For simplicity, we focus on the lateral size dependence by fixing the thickness to a moderate 60 nm, at which both the relaxation of substrate clamping and the strain transfer remain effective, since the lateral size is critically important for high-density devices.^{45,46} Nevertheless, in practical device designs, the lateral size, the thickness (including the critical value), and more importantly, their corresponding aspect ratio must be carefully engineered to obtain a significant voltage-driven magnetic domain switching (see discussions in Sec. IV).

We now discuss the correlation between the as-grown FE and magnetic domain structures in such a heterostructured island. Recent experiments have demonstrated that local magnetic domain morphology can be imprinted by the FE domain pattern underneath via strain.^{47–49} For example, the domain states in an as-grown magnetic thin film (several nanometers of thickness) could copy the ferroelastic domain patterns of the bottom FE bulk substrate (normally at a micrometer or millimeter size) due to strain transfer during magnetic thin film growth.^{45,46} In such a film-on-bulk-substrate heterostructure, the sizes of the FE and magnetic domains are comparable to each other based on the scaling law for ferroic domains (the domain width is proportional to the square root of the thickness of ferromagnets,^{50,51} ferroelastics,^{52,53} and ferroelectrics^{54,55}) and the intrinsically smaller FE domain (wall) width.⁵⁶ This would lead to an intimate elastic-coupling between the magnetic and FE domain walls.⁵⁷ However, for the magnetic and FE layers of similar thicknesses in a multiferroic island wherein the FE domain (wall) width is typically smaller than that of magnets, such one-to-one domain pattern transfer is not expected.

The domain states of the as-grown magnetic island may be determined by the average strains arising from the surface

ferroelastic domain pattern of the FE island underneath. These average strains can be obtained from the residual structural strains when the FE island is cooled down from their paraelectric (PE) state (see Sec. II). For illustration, a (001)-oriented BaTiO₃(BTO) island is taken as the representative FE material, while a soft (001)-oriented Co₂₀Fe₆₀B₂₀(CoFeB) alloy is taken as the magnetic layer due to its wide use in state-of-the-art magnetic tunnel junctions³⁷ with record high tunneling magnetoresistance of more than 1000%.⁵⁷ By taking the material parameters from literature,^{35,37,57} typical as-grown magnetic and FE domain structures in the multiferroic islands upon various types of mechanical constraints (e.g., compression or tension) from the bottom substrate/electrode are shown in Fig. 2. Herein the same notations are used to represent the magnetic and FE domains. Specifically, polarizations (or magnetizations) along the $[100]_p$, $[\bar{1}00]_p$, $[010]_p$, $[0\bar{1}0]_p$, $[001]_p$, $[00\bar{1}]_p$ directions of the cubic PE phases (or unstrained cubic magnets) are labeled as a_1^+ , a_1^- , a_2^+ , a_2^- , c^+ , c^- domain, respectively, where the subscript p indicates pseudo-cubic index. Other domains are labeled as either orthorhombic O_{12} , O_{13} , O_{23} with two non-zero vector components [e.g., O_{12} denotes magnetic $(M_1, M_2, 0)$ and FE $(P_1, P_2, 0)$] or rhombohedral (R) with all three non-zero components, i.e., $[(M_1, M_2, M_3)$ or $(P_1, P_2, P_3)]$, and we only label several of them for simplicity (see Fig. 2).

The BTO islands with various lateral sizes shown in Fig. 2(a) are subjected to an identical in-plane biaxial isotropic strain of 0.2% imposed by the underlying substrate/electrode. Such a tensile strain, albeit with considerable relaxation, would further favor the presence of in-plane a domain in the BTO³⁵ island when it cools down from the PE state to the FE state and hence produce more in-plane tensile structural-distortion. Such a residual transformation strain can then be transferred to the as-grown magnetic layer and change the magnetic domain states accordingly.^{47,48} For simplicity, we assume a full residual strain transfer, though the actual transfer would be less in a real sample due to the imperfect interface.⁴⁸ Among the three sizes considered, the $128 \times 128 \times 60 \text{ nm}^3$ BTO island exhibits the largest initial average strain of around 0.146% based on its dominative in-plane a_1 and a_2 domains despite their complex morphologies [see Fig. 2(a)], which can be further attributed to the weakest in-plane electrostatic (depolarization) energy (Sec. II) as well as the strongest substrate clamping therein [Fig. 1(c)]. Upon such tensile structural strain, an in-plane vortex-type domain state appears in the upper (001) CoFeB layer, and no one-to-one domain pattern transfer is observed as expected. In comparison, the $64 \times 64 \times 60 \text{ nm}^3$ and $32 \times 32 \times 60 \text{ nm}^3$ BTO islands with weaker substrate constraints exhibit remarkably smaller fractions of in-plane a domains mainly due to the stronger in-plane electrostatic energy, and therefore much smaller initial in-plane structural strains of 0.072% and 0.035%, respectively. Because of such weak elastic anisotropy, the domain structures in the magnetic layers would mostly depend on their respective magneto-static (shape) anisotropic energies. For example, in the almost cube-shaped $32 \times 32 \times 30 \text{ nm}^3$ CoFeB layer, a well-defined layered magnetic domain structure is exhibited

[Fig. 2(a)], with a perpendicular c and tilting O_{23}/O_{13} domains in the vicinity of magnetic-FE interface and an in-plane uniform a domain at the surface, whereas the $64 \times 64 \times 30 \text{ nm}^3$ CoFeB layer with a bit larger aspect ratio presents a fully in-plane domain structure with 90° domain wall [Fig. 2(a)].

Compared to the case of tensile substrate strain, the BTO islands show more perpendicular FE c domains upon zero substrate strain [Fig. 2(b)] and even more under the compressive substrate strain of isotropic (-0.2% , -0.2%) [Fig. 2(c)]. Take the smallest $32 \times 32 \times 60 \text{ nm}^3$ BTO island for example, an initial uniform c^- single-domain is exhibited in both cases. The presence of FE c domain would cause remarkable in-plane compressive structural-distortion that can be transferred to the as-grown magnetic thin films. As a result, perpendicular magnetic c domains would be induced in the CoFeB layer with a positive magnetostriction. Table I summarizes the residual in-plane structural strains ε_{11} in BTO islands of different lateral sizes under various substrate strains. As seen, the magnitude of residual strains decreases with increasing lateral size for the cases of zero and compressive substrate strains while increases for the case of tensile substrate strains. Both can be attributed to the preferential FE in-plane a domain in BTO islands of larger lateral size with weaker in-plane electrostatic energy and stronger substrate clamping, which would make the residual strains in BTO islands more positive. Thus, such modulation of residual structural strains in FE islands via engineering their geometric sizes and the underlying substrate, associated with a careful control over the shape of the magnet, should allow us to obtain designed initial magnetic domain states.

IV. VOLTAGE-DRIVEN PERPENDICULAR MAGNETIC DOMAIN SWITCHING

Now turn to the voltage actuated perpendicular (i.e., from in-plane to out-of-plane, and vice versa) magnetic domain switching in such multiferroic nanoislands. As the first example, in a $32 \times 32 \text{ nm}^2$ multiferroic CoFeB/BTO island, the CoFeB layer exhibits a uniform c (c^+ or c^-) single-domain throughout the voltage sequence, as shown in Fig. 3(a) and with typical domain structures illustrated in Fig. 3(b). Such perpendicular domain can readily be stabilized in such a cube-shaped nanomagnet (i.e., $32 \times 32 \times 30 \text{ nm}^3$) with almost degenerate shape anisotropy along its three principle axes. More importantly, it is induced by the large, mostly negative in-plane strain $\varepsilon_{11}(\approx \varepsilon_{22})$ of up to -0.3% [see Fig. 3(c)] based on the ferroelastic $a_1(a_2)$ to c domain switching in the bottom $32 \times 32 \times 60 \text{ nm}^3$ BTO islands.

TABLE I. The residual strains ε_{11} in as-grown BTO islands of different lateral sizes upon relaxed substrate-imposed isotropic compressive, zero, and tensile strains.

	(-0.2% , -0.2%)	(0, 0)	(0.2% , 0.2%)
$32 \times 32 \times 60 \text{ nm}^3$	-0.217%	-0.19%	0.035%
$64 \times 64 \times 60 \text{ nm}^3$	-0.202%	-0.162%	0.072%
$128 \times 128 \times 60 \text{ nm}^3$	-0.178%	-0.08%	0.146%

Such compressive in-plane strains are mainly determined by the large in-plane electrostatic energy in the $32 \times 32 \times 60 \text{ nm}^3$ BTO islands which suppresses the formation of in-plane a domain, as demonstrated by the relatively small volume fraction of FE a domain even at the coercive voltage [point B in Fig. 3(b)]. On the other hand, the substrate strain can also modify the electromechanical strains [Fig. 3(c)], but very slightly because of the remarkable relaxation [Fig. 1(c)]. As shown in Fig. 3(c), the $32 \times 32 \times 60 \text{ nm}^3$ BTO island upon the tensile substrate strain of (0.2% , 0.2%) has a larger change in the in-plane strain ε_{11} of about 0.27% than those upon zero and compressive (-0.2% , -0.2%) strains, owing to the more favorable in-plane a domain at the coercive voltage which could stretch the in-plane lattice with a resultant positive ε_{11} (i.e., about 0.007% at point B). Such favorable FE a domain can also facilitate the polarization reversal by providing more nucleation sites for a reverse FE domain growth, with concomitant slight reduction of FE coercive voltage [Fig. 3(c)].

In comparison with the stable perpendicular c domain in the cube-shaped $32 \times 32 \times 30 \text{ nm}^3$ CoFeB film which is insensitive to external voltage [Fig. 3(a)], a well-defined butterfly-shaped c domain fraction vs. voltage loop is obtained in the $64 \times 64 \times 30 \text{ nm}^3$ CoFeB layer grown on a $64 \times 64 \times 60 \text{ nm}^3$ BTO island [Fig. 4(a)], and the magnetic domain structure can be repeatedly switched between an in-plane and perpendicular direction, as directly illustrated in Fig. 4(b). Specifically, the CoFeB layer shows the largest c domain fraction change of around 53.8% when the BTO island is subjected to a tensile substrate strain of (0.2% , 0.2%) [Fig. 4(a)], as compared to the cases of zero and compressive substrate strains. A typical perpendicular striped domain for soft magnets⁵⁸ is exhibited at both the remnant and saturation states [i.e., points A and C in Fig. 4(b), respectively], the magnetic domain structure at the coercive voltage [point B in Fig. 4(b)] is almost fully in-plane. Such voltage-induced repeatable formation and annihilation of the magnetic stripes has been observed in a continuous soft Ni film grown on bulk BTO via magnetic force microscopy (MFM).⁵⁹ The obtained largest perpendicular magnetic domain switching corresponds to the highest in-plane strain change of about 0.33% [see Fig. 4(c)] under the tensile substrate strain of (0.2% , 0.2%).

Such an in-plane electromechanical strain change in the $64 \times 64 \times 60 \text{ nm}^3$ BTO is also larger than the 0.27% in the $32 \times 32 \times 60 \text{ nm}^3$ BTO [Fig. 3(c)], mainly due to the significantly larger tensile (positive) ε_{11} of 0.09% at the coercive voltage [point B in Fig. 4(c)]. This enhancement results from the notably more in-plane FE a domain at the coercivity [point B in Fig. 4(b)], which further owes to the stronger tension-type substrate clamping and the smaller in-plane electrostatic energy in the $64 \times 64 \times 60 \text{ nm}^3$ BTO with a larger aspect ratio. Likewise, the propensity of forming FE a domain at the coercive voltage can facilitate the polarization reversal, though the corresponding FE domain structure is highly unstable with polarization charge segregations at the “head to head” or “tail to tail” domain walls due to the short-time-duration voltage signals (Sec. II). This is also evidenced by the remarkably decreasing coercive voltage from ± 0.84

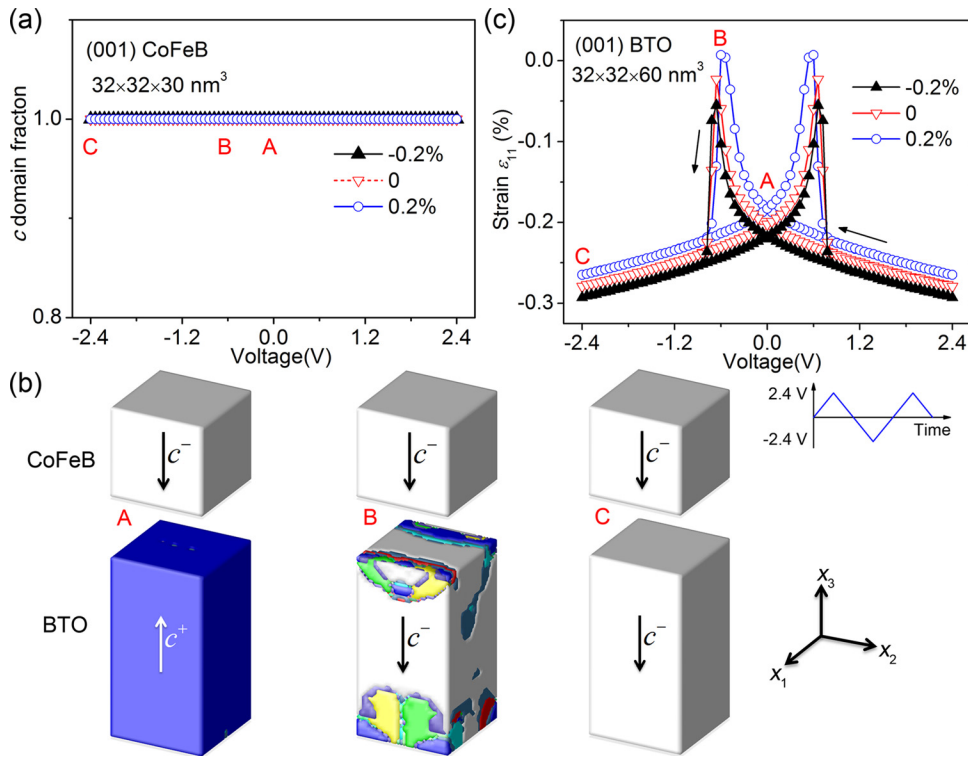


FIG. 3. Voltage-induced changes in (a) the volume fraction of perpendicular c (c^+ , c^-) domain in $32 \times 32 \times 30 \text{ nm}^3$ magnetic CoFeB layer and (c) the in-plane strain ϵ_{11} in the $32 \times 32 \times 60 \text{ nm}^3$ BTO island under substrate strains of $(-0.2\%, -0.2\%)$, $(0,0)$, and $(0.2\%, 0.2\%)$, respectively. (b) Magnetic (the first row) and FE (the second row) domain structure evolutions at Points A (remnant state), B (coercivity), and C (saturation) upon a tensile substrate strain of $(0.2\%, 0.2\%)$ on the BTO islands. The arrows indicate the magnetic or FE domain orientations.

to $\pm 0.48 \text{ V}$ [Fig. 4(c)] when the substrate strain changes from compressive $(-0.2\%, -0.2\%)$ to tensile $(0.2\%, 0.2\%)$.

Furthermore, it is worth noting that the magnetic c domain fraction in the CoFeB layer shows significant fluctuation when the actuation voltage exceeds the FE coercivity [Fig. 4(a)] irrespective of the relatively smooth variation of corresponding electromechanical strains [Fig. 4(c)]. Such fluctuation in the magnetic domain states indicates a combined magnetization switching behavior of both the processional rotation and domain-wall motion^{45,46} in the $64 \times 64 \times 30 \text{ nm}^3$ CoFeB layer. It also demonstrates an

intrinsically slower magnetic domain evolution (e.g., switching and coarsening) than the polarization switching⁶⁰ when the size of the ferroelectrics and magnets are comparable to each other. Further regarding the short time span for the strain transfer across the interface and achieving mechanical equilibrium,⁴⁵ the whole dynamic voltage-driven magnetic domain switching process in such a heterostructured nanoisland would mainly depend on the magnetic domain dynamics under electromechanical strains. Besides, the substrate strain imposed on the BTO islands also influences the evolution of magnetic domains. For the case of compressive

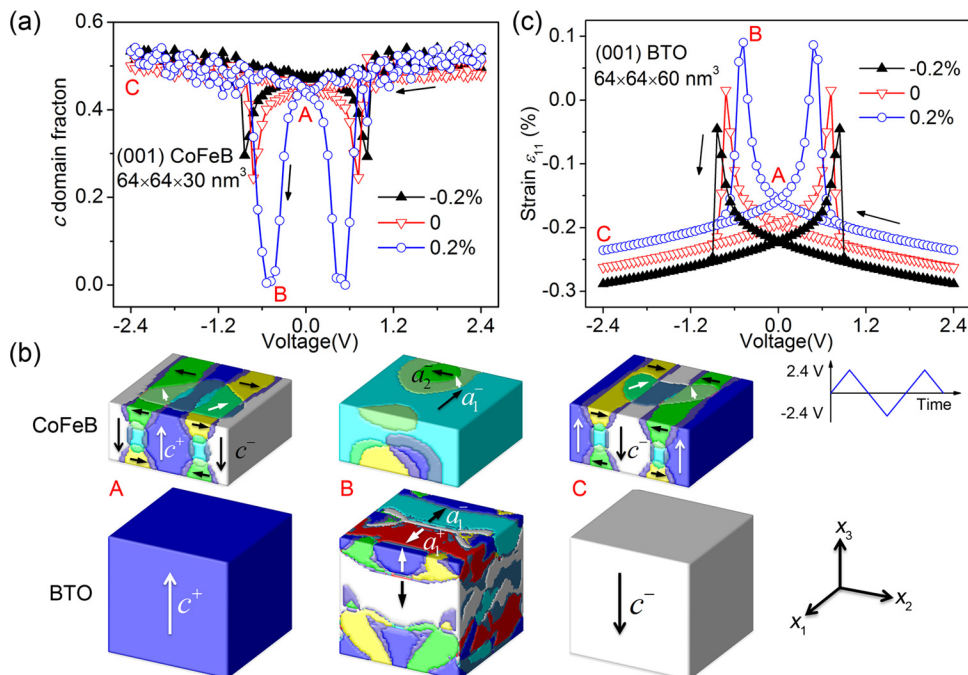


FIG. 4. Voltage-induced changes in (a) the volume fraction of perpendicular c (c^+ , c^-) domain in $64 \times 64 \times 30 \text{ nm}^3$ magnetic CoFeB layer and (c) in-plane strain ϵ_{11} in the $64 \times 64 \times 60 \text{ nm}^3$ BTO island under substrate strains of $(-0.2\%, -0.2\%)$, $(0,0)$, and $(0.2\%, 0.2\%)$, respectively. (b) Magnetic (the first row) and FE (the second row) domain structure evolutions at Points A (remnant state), B (coercivity), and C (saturation) upon a tensile substrate strain of $(0.2\%, 0.2\%)$ on the BTO islands. The arrows indicate the magnetic or FE domain orientations.

substrate strain, the magnetic c domain fraction in the $64 \times 64 \times 30 \text{ nm}^3$ CoFeB layer changes sharply from 0.296 to 0.48 [Fig. 4(a)] when the voltage increases from -0.84 V (coercivity) to -0.9 V , which happens within less than 0.5 ns (see Sec. II). Such a prompt switching corresponds to the abrupt change of the electromechanical strain ε_{11} at the coercive voltage [Fig. 4(c)]. By contrast, the strain value changes gradually around the coercive voltage for the cases of zero and tensile substrate strains due to the preferential in-plane FE a domain therein with associated smooth polarization reversal. Accordingly, the magnetic domain structures evolve gradually in both cases.

In multiferroic CoFeB/BTO islands with an even larger lateral size of 128 nm , the islands under zero substrate strain present the largest voltage-driven change in the magnetic c domain fraction of about 37.3% among all three substrate strains [Fig. 5(a)]. By comparison, although the tensile substrate strain of $(0.2\%, 0.2\%)$ leads to a bit more in-plane FE a domain [point B in Fig. 5(b)] and thus a slightly more positive (tensile) value of ε_{11} at the coercive voltage [point B in Fig. 5(c)], the value of in-plane compressive strain at the saturation voltage [point C in Fig. 5(c)] is reduced by a greater extent because of the even stronger tension-type substrate clamping which suppresses the out-of-plane ferroelastic a to c switching. Accordingly, the overall in-plane strain change becomes smaller, leading to a smaller voltage-induced perpendicular magnetic domain switching under the tensile substrate strain with typical magnetic domain structures presented in Fig. 5(b). As illustrated, an explicit in-plane magnetic vortex appears at the remnant state (point A), which would somewhat expand when the voltage approaches the coercivity (point B) with tensile in-plane strains, and then gradually decomposes due to the growth of perpendicular c domain which penetrates the magnetic layer longitudinally at the saturation state (point C) with compressive in-plane strains. Furthermore, compared to the remarkable

domain fluctuations in $64 \times 64 \times 30 \text{ nm}^3$ CoFeB layer [Fig. 4(a)], the magnetic domain structures stabilize much faster herein with a relatively smooth variation trend upon voltages [Fig. 5(a)]. This can be attributed to the increased volume fraction of domain walls in the larger $128 \times 128 \times 60 \text{ nm}^3$ CoFeB with dominative magnetization switching behavior via domain-wall motion, which is intrinsically faster than the processional magnetization rotation.^{45,46}

In addition, the voltage-driven magnetic c domain fraction change (about 31.8%) in the $128 \times 128 \text{ nm}^2$ CoFeB/BTO islands under tensile substrate strain is significantly smaller than its $64 \times 64 \text{ nm}^2$ counterpart (about 53.8%), mainly because of the smaller in-plane strain change. Such decreasing strain change with increasing lateral size is mainly determined by the less negative (compressive) value of ε_{11} at saturation voltage (point C) of about -0.208% (128 nm) caused by the enhanced tension-type substrate clamping. Moreover, the tensile ε_{11} at the coercive voltage (point B) also shows a moderate decrease from 0.09% (64 nm) to 0.06% (128 nm) possibly due to the increased volume fractions of domain walls and orthorhombic domain in larger FE islands [e.g., the O_{13} phase at Point B in Fig. 5(b)], irrespective of the larger in-plane electrostatic energy in the $128 \times 128 \times 60 \text{ nm}^3$ BTO islands which should lead to more in-plane FE a domain.

For the case of compression-type substrate clamping, the voltage-driven changes in the in-plane electromechanical strain and corresponding magnetic c domain fraction in the larger CoFeB/BTO island of $128 \times 128 \text{ nm}^2$ are also smaller [Fig. 5(a)]. However, the only exception arises for the case of zero substrate strain, where the maximum in-plane strain change increases caused by a remarkable increase in ε_{11} at the coercive voltage from 0.015% (64 nm) to 0.053% (128 nm) and a moderate decrease at the saturation voltage [see Figs. 4(c) and 5(c)]. Both changes are mainly attributed to the smaller in-plane electrostatic energy and the resultant

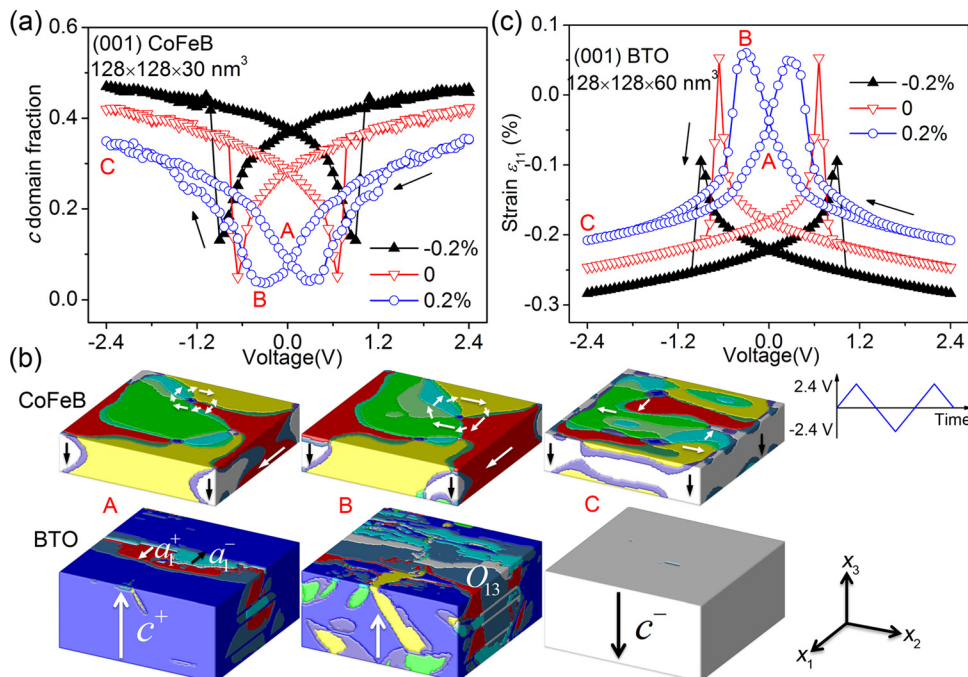


FIG. 5. Voltage-induced changes in (a) the volume fraction of perpendicular c (c^+ , c^-) domain in $128 \times 128 \times 30 \text{ nm}^3$ magnetic CoFeB layer and (c) in-plane strain ε_{11} in the $128 \times 128 \times 60 \text{ nm}^3$ BTO island under substrate strains of $(-0.2\%, -0.2\%)$, $(0, 0)$, and $(0.2\%, 0.2\%)$, respectively. (b) Magnetic (the first row) and FE (the second row) domain structure evolutions at Points A (remnant state), B (coercivity), and C (saturation) upon a tensile strain of $(0.2\%, 0.2\%)$ on the BTO islands. The arrows indicate the magnetic or FE domain orientations.

more FE a domain, since contribution from the elastic energy is negligible under zero substrate strain. Figure 6 displays the maximum voltage-induced changes in the magnetic c domain fraction Δf_c and the in-plane electromechanical strains $\Delta \varepsilon_{11}$, and the FE coercive voltage V_c in the CoFeB/BTO nanoislands as a function of the lateral size under various substrate constraints.

Thus, in such multiferroic magnetic-FE nanoislands, the voltage-driven magnetic domain switching is determined by the geometric size of a specific magnetic layer, the ferroelastic domain pattern of the FE island underneath with structural residual strains (Table I) that can be transferred to the as-grown magnetic thin films and further change the initial magnetic domain states (Fig. 2), and the dynamic electromechanical strains imposed on it [Figs. 3(c), 4(c), and 5(c)]. Such electromechanical strains are further governed by the size of the FE island which would lead to different electrostatic energy contributions and various levels of mechanical relaxations [Fig. 1(c)], as well as the type of mechanical constraint from the bottom substrate. As shown in Figs. 6(a) and 6(b), the $64 \times 64 \text{ nm}^2$ multiferroic island under a tensile substrate strain of (0.2%, 0.2%) exhibits the largest in-plane strain change $\Delta \varepsilon_{11}$ of 0.33% and the resultant magnetic c domain fraction change Δf_c of 53.8%. This might indicate that the lateral size of the multiferroic island can neither be too big nor too small to maximize the voltage-driven magnetic domain switching under a given thickness. If the lateral size is too small, the enhanced in-plane magnetostatic and electrostatic energy would lead to a favorable perpendicular c domain in both the magnetic and FE layers. Particularly, these dipole-dipole energy contributions could be dominant, making the domain states very difficult to be modulated by external electromechanical strains, for instance, the $32 \times 32 \text{ nm}^2$ CoFeB/BTO island exhibits little voltage-driven change in the magnetic c domain fraction [Fig. 6(a)]. In addition, the remarkable mechanical relaxation in small FE islands would make both the in-plane strain change $\Delta \varepsilon_{11}$ [Fig. 6(b)] and the FE coercive voltage V_c [Fig. 6(c)]

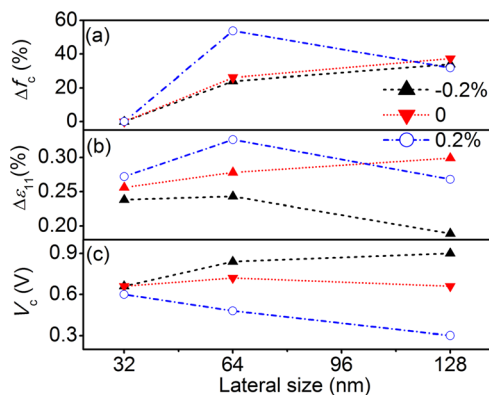


FIG. 6. Lateral size (length and width) dependence of the maximum voltage-driven changes in (a) the perpendicular magnetic c (i.e., c^+ plus c^-) domain fraction change Δf_c and (b) the in-plane electromechanical strain $\Delta \varepsilon_{11}$; (c) the ferroelectric coercive voltage V_c . The multiferroic CoFeB/BTO nanoislands are subjected to substrate-imposed in-plane strains of compressive (-0.2%, 0.2%), zero, and tensile (0.2%, 0.2%), respectively. The thicknesses of the CoFeB and BTO layers are set as 30 nm and 60 nm, respectively.

relatively insensitive to the substrate strains, which would somewhat lose design flexibility. On the other hand, if the lateral size is too large, the strong substrate clamping would inhibit large in-plane electromechanical strain changes and the resultant voltage-driven magnetic domain switching. For example, the $\Delta \varepsilon_{11}$ in the larger $128 \times 128 \text{ nm}^2$ CoFeB/BTO islands decreases remarkably upon both the compressive and tensile substrate strains [Fig. 6(b)]. Nevertheless, despite such decrease in the $\Delta \varepsilon_{11}$ upon the compressive substrate strain, the corresponding voltage-induced magnetic domain fraction change Δf_c moderately increases [Fig. 6(a)], which is mainly attributed to the weaker in-plane magnetostatic (demagnetization) energy in the larger $128 \times 128 \times 30 \text{ nm}^2$ CoFeB film with significantly smaller magnetic c domain fraction at the coercive voltage [see Point B in Figs. 4(a) and 5(a)].

Therefore, in such heterostructured nanoislands, the geometric sizes of both magnetic and FE layers, as well as the bottom electrode/substrate layer must be carefully designed to make the best use of the magnetostatic/electrostatic energy and substrate constraint without making them mutually exclusive. In practical device designs, these two aspects should be further considered together with other size-dependent factors such as thermal stability⁶¹ and ferroelastic relaxation.³⁰ Nevertheless, our simulations show that the lateral size of 64 nm could be a compromised lateral size for a large voltage-driven magnetic domain switching.

V. CONCLUSIONS

Large voltage-induced perpendicular magnetic domain switching can be realized in a magnetic-FE nanoisland structure, which was previously limited by substrate-imposed in-plane clamping in continuous multiferroic layered composite thin films.⁶² Thus such a three-dimensional multiferroic nanoisland structure offers an interesting platform for the design of novel microelectronic and/or spintronic devices with purely electrically driven means.⁸ This is not just because of its physically small size suitable for high-density device applications, but also for the controllable manner of relieving the lateral substrate constraint which can provide great design flexibility. Fundamentally, the convergence of nanoscale magnetism, ferroelectricity, and ferroelasticity in such a multiferroic nanoisland structure should enable novel coupling behaviors at the interface, and our phase-field method should be particularly useful in the design of novel devices as well as illustrating the dynamic evolution processes of both magnetic and FE domains upon external (e.g., magnetic, electric, elastic) fields with elegant treatments on the complex mechanical, magnetostatic, and electrostatic boundary conditions.

ACKNOWLEDGMENTS

This work was supported by the National Basic Research Program of China (Grant No. 2009CB623303), the NSF of China (Grant Nos. 11234005 and 50921061), and the NSF (Grant No. DMR-1006541). The computer simulations were carried out on the LION and Cyberstar clusters at the

Pennsylvania State University supported in part by NSF Major Research Instrumentation Program through grant OCI-0821527 and in part by the Materials Simulation Center and the Graduated Education and Research Services at the Pennsylvania State University.

- ¹D. D. Awschalom and M. E. Flatte, *Nat. Phys.* **3**, 153 (2007).
- ²J. G. Zhu, *Proc. IEEE* **96**, 1786 (2008).
- ³J. Sinova and I. Žutić, *Nature Mater.* **11**, 368 (2012).
- ⁴C. Chappert, A. Fert, and F. N. Van Dau, *Nature Mater.* **6**, 813 (2007).
- ⁵J. C. Slonczewski, *J. Magn. Magn. Mater.* **159**, L1 (1996).
- ⁶A. Brataas, A. D. Kent, and H. Ohno, *Nature Mater.* **11**, 372 (2012).
- ⁷Y. M. Huai, *AAPPS Bull.* **18**, 33 (2008).
- ⁸H. Ohno, *Nature Mater.* **9**, 952 (2010).
- ⁹D. Chiba, M. Sawicki, Y. Nishitani, Y. Nakatani, F. Matsukura, and H. Ohno, *Nature (London)* **455**, 515 (2008).
- ¹⁰T. Maruyama *et al.*, *Nat. Nanotechnol.* **4**, 158 (2009).
- ¹¹W. Eerenstein, N. D. Mathur, and J. F. Scott, *Nature (London)* **442**, 759 (2006).
- ¹²R. Ramesh and N. A. Spaldin, *Nature Mater.* **6**, 21 (2007).
- ¹³J. Ma, J. Hu, Z. Li, and C.-W. Nan, *Adv. Mater.* **23**, 1062 (2011).
- ¹⁴T. Cai, S. Ju, J. Lee, N. Sai, A. A. Demkov, Q. Niu, Z. Li, J. Shi, and E. Wang, *Phys. Rev. B* **80**, 140415 (2009).
- ¹⁵C.-G. Duan, S. S. Jaswal, and E. Y. Tsymlal, *Phys. Rev. Lett.* **97**, 047201 (2006).
- ¹⁶V. Garcia *et al.*, *Science* **327**, 1106 (2010).
- ¹⁷J. D. Burton and E. Y. Tsymlal, *Phys. Rev. B* **80**, 174406 (2009).
- ¹⁸C. A. F. Vaz, J. Hoffman, Y. Segal, J. W. Reiner, R. D. Grober, Z. Zhang, C. H. Ahn, and F. J. Walker, *Phys. Rev. Lett.* **104**, 127202 (2010).
- ¹⁹P. Yu *et al.*, *Phys. Rev. Lett.* **105**, 027201 (2010).
- ²⁰W. Eerenstein, M. Wiora, J. L. Prieto, J. F. Scott, and N. D. Mathur, *Nature Mater.* **6**, 348 (2007).
- ²¹C. Thiele, K. Dörr, O. Bilani, J. Rödel, and L. Schultz, *Phys. Rev. B* **75**, 054408 (2007).
- ²²V. Skumryev *et al.*, *Phys. Rev. Lett.* **106**, 057206 (2011).
- ²³S. M. Wu, S. A. Cybart, P. Yu, M. D. Rossell, J. X. Zhang, R. Ramesh, and R. C. Dynes, *Nature Mater.* **9**, 756 (2010).
- ²⁴L. Q. Chen, *Ann. Rev. Mater. Res.* **32**, 113 (2002).
- ²⁵L. Q. Chen, *J. Am. Ceram. Soc.* **91**, 1835 (2008).
- ²⁶A. Chanthbouala *et al.*, *Nature Nanotechnol.* **7**, 101 (2012).
- ²⁷J. X. Zhang, G. Sheng, and L. Q. Chen, *Appl. Phys. Lett.* **96**, 132901 (2010).
- ²⁸J.-M. Hu and C. W. Nan, *Phys. Rev. B* **80**, 224416 (2009).
- ²⁹C.-W. Nan, G. Liu, Y. Lin, and H. Chen, *Phys. Rev. Lett.* **94**, 197203 (2005).
- ³⁰S. H. Baek, H. W. Jang, C. M. Folkman, Y. L. Li, B. Winchester, J. X. Zhang, Q. He, Y. H. Chu, C. T. Nelson, M. S. Rzechowski, X. Q. Pan, R. Ramesh, L. Q. Chen, and C. B. Eom, *Nature Mater.* **9**, 309 (2010).
- ³¹X. Ren, *Nature Mater.* **3**, 91 (2004).
- ³²Y. L. Li, S. Y. Hu, Z. K. Liu, and L. Q. Chen, *Appl. Phys. Lett.* **81**, 427 (2002).
- ³³Y. L. Li, L. Q. Chen, G. Asayama, D. G. Schlom, M. A. Zurbuchen, and S. K. Streiffer, *J. Appl. Phys.* **95**, 6332 (2004).
- ³⁴J. X. Zhang, R. Wu, S. Choudhury, Y. L. Li, S. Y. Hu, and L. Q. Chen, *Appl. Phys. Lett.* **92**, 122906 (2008).
- ³⁵Y. L. Li and L. Q. Chen, *Appl. Phys. Lett.* **88**, 072905 (2006).
- ³⁶C. A. F. Vaz *et al.*, *Rep. Prog. Phys.* **71**, 056501 (2008).
- ³⁷S. Ikeda *et al.*, *Nature Mater.* **9**, 721 (2010).
- ³⁸A. G. Khachaturyan, *Theory of Structural Transformation in Solids* (Wiley, New York, 1983).
- ³⁹A. N. Stroh, *J. Math. Phys.* **41**, 77 (1962).
- ⁴⁰J.-M. Hu, G. Sheng, J. X. Zhang, C. W. Nan, and L. Q. Chen, *J. Appl. Phys.* **109**, 123917 (2011).
- ⁴¹J. X. Zhang and L. Q. Chen, *Acta Mater.* **53**, 2845 (2005).
- ⁴²M. E. Schabes and A. Aharoni, *IEEE Trans. Magn.* **23**, 3882 (1987).
- ⁴³L. Q. Chen and J. Shen, *Comput. Phys. Commun.* **108**, 147 (1998).
- ⁴⁴N. A. Pertsev, H. Kohlstedt, and B. Dkhil, *Phys. Rev. B* **80**, 054102 (2009).
- ⁴⁵J.-M. Hu, Z. Li, L.-Q. Chen, and C.-W. Nan, *Nat. Commun.* **2**, 553 (2011).
- ⁴⁶J.-M. Hu, Z. Li, L.-Q. Chen, and C.-W. Nan, *Adv. Mater.* **24**, 2869 (2012).
- ⁴⁷T. H. E. Lahtinen, J. O. Tuomi, and S. van Dijken, *Adv. Mater.* **23**, 3187 (2011).
- ⁴⁸T. H. E. Lahtinen, K. J. A. Franke, and S. van Dijken, *Sci. Rep.* **2**, 258 (2012).
- ⁴⁹R. V. Chopdekar *et al.*, *Phys. Rev. B* **86**, 014408 (2012).
- ⁵⁰L. Laudau and E. Lifshitz, *Phys. Z. Sowjetunion* **8**, 153 (1935).
- ⁵¹C. Kittel, *Phys. Rev.* **70**, 965 (1946).
- ⁵²T. Mitsui and J. Furuichi, *Phys. Rev.* **90**, 193 (1953).
- ⁵³A. L. Roitburd, *Phys. Status Solidi A* **37**, 329 (1976).
- ⁵⁴A. Kopal, T. Bahnik, and J. Fousek, *Ferroelectrics* **202**, 267 (1997).
- ⁵⁵G. Catalan, H. Béa, S. Fusil, M. Bibes, P. Paruch, A. Barthélémy, and J. F. Scott, *Phys. Rev. Lett.* **100**, 027602 (2008).
- ⁵⁶K. J. A. Franke, T. H. E. Lahtinen, and S. van Dijken, *Phys. Rev. B* **85**, 094423 (2012).
- ⁵⁷S. Ikeda, J. Hayakawa, Y. Ashizawa, Y. M. Lee, K. Miura, H. Hasegawa, M. Tsunoda, F. Matsukura, and H. Ohno, *Appl. Phys. Lett.* **93**, 082508 (2008).
- ⁵⁸A. Hubert and R. Schäfer, *Magnetic Domains* (Springer, Berlin, 1998).
- ⁵⁹M. Ghidini, R. Pellicelli, J. L. Prieto, X. Moya, J. Soussi, J. Briscoe, S. Dunn, and N. D. Mathur, *Nat. Commun.* **4**, 1453 (2013).
- ⁶⁰P. P. Horley, A. Sukhov, C. Jia, E. Martínez, and J. Berakdar, *Phys. Rev. B* **85**, 054401 (2012).
- ⁶¹R. F. L. Evans, R. W. Chantrell, U. Nowak, A. Lyberatos, and H. J. Richter, *Appl. Phys. Lett.* **100**, 102402 (2012).
- ⁶²H. Zheng, J. Wang, S. E. Lofland, Z. Ma, L. Mohaddes-Ardabili, T. Zhao, L. Salamanca-Riba, S. R. Shinde, S. B. Ogale, F. Bai, D. Viehland, Y. Jia, D. G. Schlom, M. Wuttig, A. Roytburd, and R. Ramesh, *Science* **303**, 661 (2004).